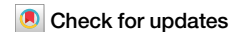
A Nature Portfolio journal



https://doi.org/10.1038/s43247-025-02951-5

Fuel sulfur content can modulate contrail ice crystal numbers



Rebecca Dischl © ¹.² , Raphael Märkl¹.², Daniel Sauer © ¹, Christiane Voigt © ¹.², Theresa Harlaß¹, Monika Scheibe © ¹, Valerian Hahn¹, Stefan Kaufmann¹, Andreas Marsing © ¹, Andreas Dörnbrack¹, Anke Roiger¹, Fangqun Yu © ³, Maxime Gauthier © ⁴, Charles Renard⁴, Peter Swann⁵, Mark Johnson⁵, Denise Ahrens⁶, Reetu Sallinen², Georg Eckel © 8 & Patrick Le Clercq © 8

In recent efforts to reduce the radiative forcing of aviation, fuel design has gained increased attention. Sustainable Aviation Fuels are seeing wider adoption, and their positive impact on carbon dioxide and non-volatile soot particle emissions is well-established. However, the effects of the reduction in fuel sulfur content on volatile particle emissions and contrails are unknown. This study presents observations from in-flight measurements of emissions and contrails of an Airbus A350-900 burning fuels with different sulfur contents. We find a reduction in volatile particles and contrail ice crystals for low-sulfur fuels. For higher fuel sulfur contents, our findings demonstrate an additional contrail ice particle source through activation of sulfate aerosols. Our data-driven results need to be consolidated by in-flight observations with different fuels and engines. Eventually, climate impact estimates as well as regulations should account for the modulating effect of the fuel sulfur content on contrail ice particle numbers.

Aviation is a growing sector and already accounts for about 3.5% of the anthropogenic radiative forcing¹. As the aviation sector strives for carbon neutrality, the adoption of sustainable aviation fuels (SAF) has emerged as a key strategy. In the European Union, the ReFuelEU Aviation Regulation mandates a gradual increase in the blending of SAFs with conventional kerosene², while in the United States, tax credits for SAF production have been introduced to incentivize its adoption³. SAFs offer a promising path for mitigating both CO₂ and non-CO₂ climate effects from aviation. Advancing regulatory frameworks requires a reduction in uncertainties related to the benefits of mitigation strategies, with the climate impact of contrails representing one of the major remaining sources of uncertainty⁴⁻⁶. Contrail cirrus produce a major part of the non-CO2 effects, warming the atmosphere with an effective radiative forcing of about 57.4 ± 40 mW m⁻² in 2018¹. Contrails form at flight altitude when the hot aircraft engine exhaust cools down to atmospheric air temperatures below −40 °C and reaches liquid saturation of water vapor within the plume as determined by the Schmidt–Appleman threshold temperature $(T_{SA})^7$. The water vapor then condenses on emitted, newly formed and in-mixed ambient aerosol particles and forms liquid droplets. For the current aircraft fleet, the exhaust aerosols generally contain non-volatile soot particles and smaller volatile aerosols. The resulting droplets freeze due to the cold temperatures at cruising altitude and form contrails. In ice-subsaturated conditions, the contrail ice crystals sublimate shortly after their formation⁸. However, in ice-supersaturated conditions, initially line-shaped contrails⁹ can spread out and form large-scale contrail cirrus clouds^{10,11}. Through trapping of outgoing longwave radiation and reflection of solar shortwave radiation¹², contrail cirrus lead to a globally averaged positive radiative forcing^{13–15}. In contrast to CO₂, contrail cirrus have an average lifetime of a few hours^{16,17}, therefore reducing the occurrence of warming contrails or changing their properties could help to quickly reduce the climate impact of aviation. This can be realized, for example, by using sustainable aviation fuels such as hydroprocessed esters and fatty acids synthetic paraffinic kerosene (HEFA-SPK) or other synthetic fuels with low aromatic contents^{18,19}. These sustainable aviation fuels cause lower soot emissions²⁰, which reduces ice crystal numbers^{21,22} and the climate forcing of the contrails^{16,23,24}.

The influence of the engine and the fuel composition, in particular the fuel sulfur content (FSC) on particle emissions was previously investigated experimentally in several projects, for example, the flight experiments with the supersonic aircraft Concorde^{25–27}, the Pollution From Aircraft Emissions in the North Atlantic Flight Corridor (POLINAT) projects²⁸, the NASA

¹Deutsches Zentrum f. Luft- und Raumfahrt, Institute of Atmospheric Physics, Oberpfaffenhofen, Bavaria, Germany. ²Johannes Gutenberg University, Institute of Atmospheric Physics, Mainz, Germany. ³Atmospheric Sciences Research Center, University at Albany, Albany, NY, 12226, USA. ⁴Airbus Operations SAS, Toulouse, France. ⁵Rolls-Royce plc., Derby, UK. ⁶Rolls-Royce Deutschland, Dahlewitz, Germany. ⁷Neste Corporation, R&D, Porvoo, Finland. ⁸Deutsches Zentrum f. Luft- und Raumfahrt, Institute of Combustion Technology, Stuttgart, Germany. ⁹Present address: NASA Postdoctoral Programm (ORAU) at NASA Langley Research Center, Hampton, VA, USA. —e-mail: rebecca.dischl@dlr.de

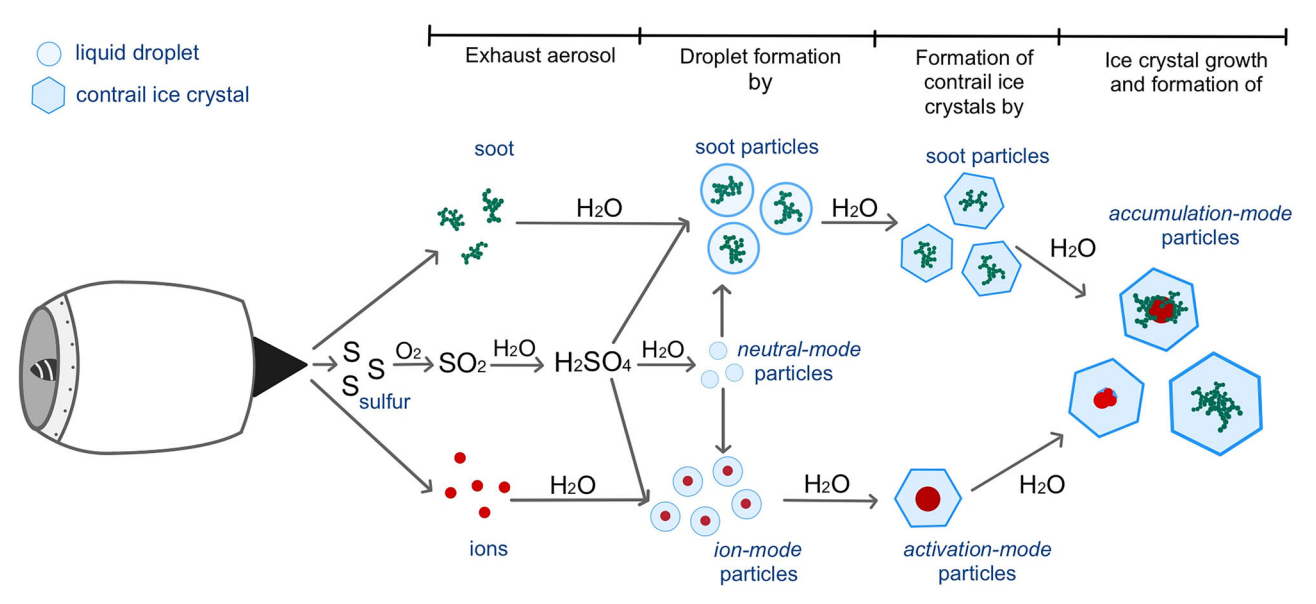


Fig. 1 | Particle and contrail formation for fuels with medium (500 ppm) to high (3000 ppm) sulfur content.

Subsonic Aircraft Contrail and Cloud Effects Special Study (SUCCESS)²⁹ and the Subsonic Assessment Near-Field Interactions Field Experiments (SNIF I–III)³⁰ as well as the SULFUR 1–7 campaign series^{31,32}. These campaigns suggested that the fuel sulfur content could have an influence on aerosol particle emissions and contrail ice particle formation. Answers on the resulting impact on contrails remained inconclusive and might have been masked by the stronger impact of the larger soot particles on contrail formation.

Today's technology strives towards reducing particle emissions, so that soot emissions below 10¹⁵ soot particles per kg of fuel are common^{20,33}. As engine technology advances and soot emissions decrease, the role of volatile particles in contrail formation becomes increasingly important. It is therefore necessary to investigate the particle formation of modern jet engines and the influence of fuel composition on volatile aerosols and the resulting contrails. Previous in-flight studies have been conducted using older engine types with substantially higher soot emissions (>2 \times 10¹⁵ per kg fuel), where the impact of fuel sulfur content was less pronounced or not observed²¹. In contrast, this study examines a modern engine fitted with a Rich-Quench-Lean (RQL) combustor, which represents the most common combustor technology listed in the ICAO Aircraft Engine Emissions Databank³⁴ and emits substantially less soot, making the influence of fuel sulfur content more discernible. The sulfur content of the fuels used in this study spans the typical range of today's fossil-based jet fuels and extends to the low sulfur levels characteristic of SAF, thereby representing a realistic spectrum of both current and future fuel compositions.

We investigate the influence of the fuel sulfur content on emitted aerosol particles and contrail formation under ambient conditions. Our analysis is based on in-flight measurements and modeling. We demonstrate that, for the tested engine, variations in fuel sulfur content have a substantial impact on both the ice activation efficiency of soot particles and the contribution of volatile aerosols to ice nucleation.

Exhaust particles and contrail formation

Conventional jet fuels have a mean FSC of 400–500 parts per million by mass (ppm), with no apparent trend in the recent years^{35,36}. Current fuel specifications permit concentrations up to 3000 ppm³⁷, which results in a broad distribution and a median FSC in the range of approximately 200–400 ppm³⁶. In contrast, SAF generally has negligible sulfur content, as they are derived from sulfur-free or sulfur-lean feedstocks.

As a result of the combustion process in the engine combustor, the fuel sulfur is converted to sulfur oxides (SO_x), which are then partially converted into gaseous sulfuric acid H_2SO_4 behind the engine ^{26,32,38}. The conversion

fraction of fuel sulfur to available sulfuric acid mainly depends on the fuel sulfur content and might be influenced by engine characteristics; it is estimated by different models and experiments to range between 0.3% and 5% ^{32,39–42}.

Due to the cooling of the exhaust air, H_2SO_4 becomes supersaturated and partially condenses along with H_2O on emitted soot particles, leading to a liquid coating of H_2SO_4 and H_2O on the surface of the soot particles⁴³. Due to the coating, the hygroscopicity and size of the soot particles are enhanced. These particles are more effective in capturing water vapor, and therefore support the formation of contrail ice crystals^{44,45}.

Volatile aerosol particles form via two main pathways (see Fig. 1): homogeneous nucleation of H₂SO₄ and H₂O forming electrically neutral aerosol clusters (neutral-mode particles); and heterogeneous nucleation, i.e., nucleation on pre-existing particles or ions (including chemiion-induced nucleation), forming ion-mode particles. During combustion, high concentrations of chemiions (CI) are generated that further react and eventually cluster with water, sulfur, and nitrogen compounds, forming these small ion-mode particles^{32,38,46,47}. Consequently, chemiions represent the dominant source of condensation nuclei (CN) leading to volatile particle formation⁴⁷. During ground experiments, a CI number emission index of about (0.2–2) × 10¹⁷ kg⁻¹ at the engine exit was determined, depending on the engine type, engine condition, and fuel composition^{48,49}. Measurements of CI concentrations and their composition from modern jet engines would be of interest.

The volatile aerosol further grows by the uptake of H_2SO_4 and $H_2O^{27,50}$. For fuel sulfur contents larger than $\sim \! 100$ ppm, sulfate compounds become the main contributor to ultrafine volatile aerosol in the aircraft exhaust 32,51 . Experiments indicate that the composition of volatile particles may be dominated by non-sulfate compounds for fuel sulfur contents below $50{\text -}100$ ppm 51 . For such fuels, species aside from H_2SO_4 , e.g. HNO_3 and organic compounds, mainly contribute to or even control the initial growth of volatile particles 39,51 .

Through scavenging, the neutral-mode clusters primarily account for the growth of ion-mode clusters during the first minutes of plume evolution⁵². The number of volatile particles in the plume is therefore not only affected by the FSC, but also by the initial number of CI²⁷. However, the amount of condensable sulfuric acid as well as temperature and relative humidity over ice (RHi) influences the growth and thus particle mass and particle diameter, and thereby the number of particles detectable by the instruments. The ion-mode particles continue to grow within the first minutes after formation²⁷. The maximum volume mean diameter of the ion-mode particles then amounts up to 5–12 nm for average to high sulfur fuels (>500 ppm)^{38,39,53}.

Table 1 | Selected properties of the fuels burned by the A350-900 during the test sequences

Fuel	Ultra-low-sulfur HEFA-SPK	Low-sulfur Jet A-1	Medium-sulfur blend fuel	ECLIF3-1 HEFA-SPK	ECLIF3-1 Jet A-1	World average Jet A-1 (2006)
Components	100%	100%	38% HEFA-SPK+	100%	100%	
	HEFA-SPK	Jet A-1	62 % Jet A-1	HEFA-SPK	Jet A-1	
Hydrogen content [%m/m]	15.18	14.25	14.39	15.11	14.08	13.89
Carbon content [%m/m]	84.82	85.74	85.56	84.89	85.90	N/A
Sulfur content [%m/m]	0.0003	0.0125	0.0505	0.0007	0.0211	0.0460
Aromatics [%v/v]	<0.1	13.4	10.8	N/A	13.4	19.2

Fuel properties were analyzed according to ASTM standards. World average fuel data were obtained from the CRC World Fuel Survey³⁵

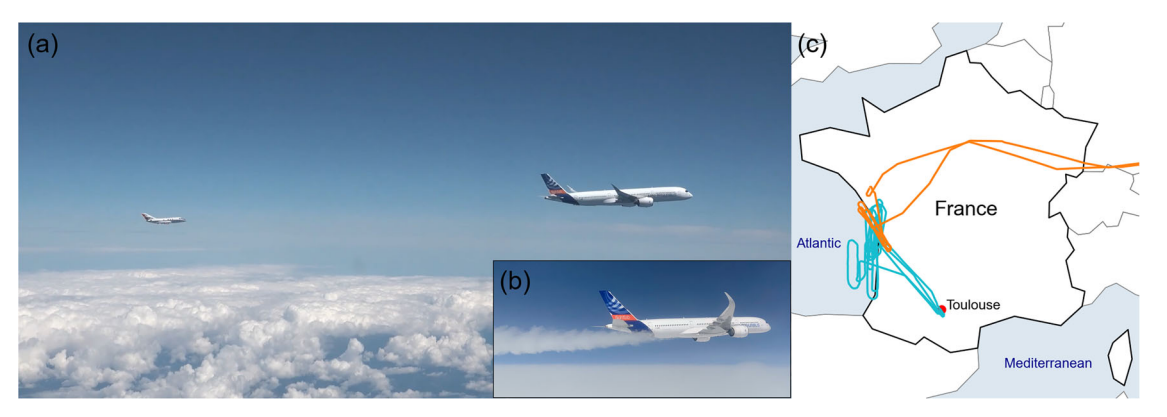


Fig. 2 | Side-view of the research aircraft Falcon and the A350–900, and flight routes of the measurement flights. The Falcon chases the A350–900 to sample a emissions and b contrails. c The emission measurement flight (orange) and the two

contrail measurement flights (blue) were performed along the French Atlantic coast in November 2021.

If contrail-forming conditions prevail in the ambient atmosphere, meaning the air temperature is below the Schmidt–Appleman threshold temperature and the air is supersaturated with respect to ice, the number of contrail ice particles is mainly determined by the number of suitable CN. For conventional engines, soot particles constitute a large fraction of CN, while the droplet-activating efficiency of the volatile aerosol is a function of its size distribution, and therefore FSC, according to the Köhler theory²⁷. Models indicate that only a fraction of the activated liquid acid droplets eventually freeze and continue to grow as contrail ice particles, since the activated soot particles freeze sooner and scavenge the available water vapor earlier³⁸. A recent study suggests that the contribution of the volatile aerosols to contrail ice is dependent on the ambient temperature, on the number of soot particles, as well as on the sizes of the soot primary particles and aggregates⁵⁴.

If contrail ice particles develop in the exhaust plume, the uptake of water vapor by ion-mode particles results in a larger activation-mode located at about 30 nm diameter. The accumulation-mode is found around 80 nm diameter and may result from sulfate aerosol formation in contrail ice particles that have scavenged vapors and other particles³⁸.

Results

During the Emission and CLimate Impact of alternative Fuels campaign (ECLIF3) in 2021, we measured the emissions of trace gases, total particles, and non-volatile particles (nvPM), and the number concentration and size distribution of contrail ice crystals from modern RQL jet engines in flight^{22,33,55}. We conducted test flights in spring (ECLIF3-1) and fall 2021 (ECLIF3-2). Measurements shown here were performed during three measurement flights in November 2021 (ECLIF3-2). We sampled the emissions of three different fuels, a HEFA-SPK with a sulfur content of 3 ppm, a conventional Jet A-1 with a sulfur content of 125 ppm and a blend fuel (containing 38% HEFA-SPK) with a sulfur content of 505 ppm. The blend fuel contained a different Jet A-1 with an increased sulfur content, resulting in a higher sulfur content of the blend fuel compared to the sampled reference

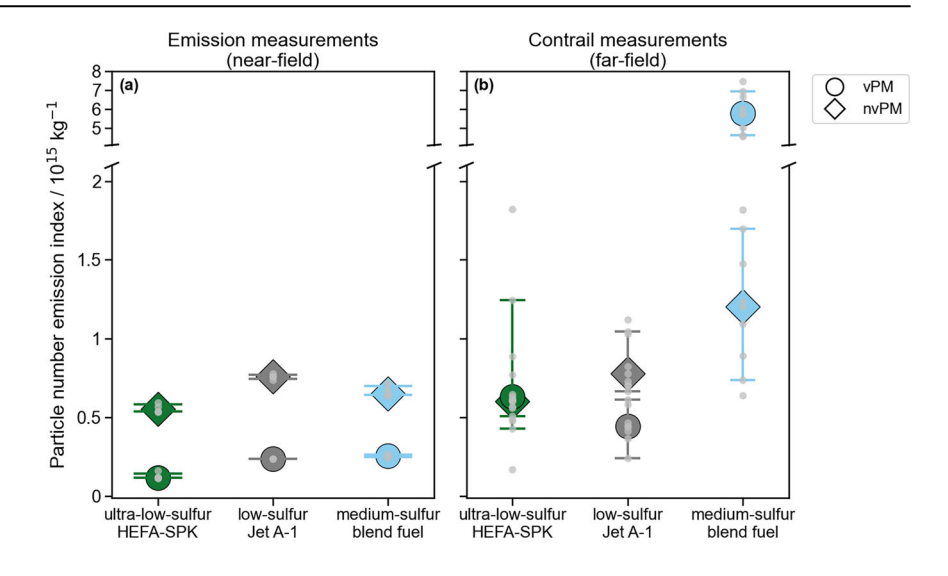
Jet A-1. The fuel composition is summarized in Table 1. With sulfur contents ranging from 3 to 505 ppm, the selected fuels reflect the composition of both current fossil-based jet fuels and anticipated SAF, enabling the analysis of the influence of the FSC under present and future operational conditions.

We measured the emissions of the leading aircraft, an Airbus A350-900 equipped with Rolls-Royce Trent XWB-84 engines, using the German Aerospace Center (DLR) research aircraft Falcon (see Fig. 2). The sample inlets for trace gas and aerosol instrumentation are mounted on the center line of the upper fuselage of the Falcon. Size distribution and number concentration of ice particles are measured with cloud particle probes mounted in underwing pods. The CO₂ measurements were used as a tracer to calculate the emission indices (EI) to scale the aerosol and ice particle emissions to the amount of fuel burned, providing a dilution-independent measure of emission (see Section "Calculation of emissions indices"). The power setting of the A350-900 engines was characterized by the parameters T30, which refers to the high-pressure compressor outlet temperature, and fuel flow (FF). The lubrication oil was vented through a separate outlet, distinct from the core exhaust, and is therefore expected to have a negligible influence on the volatile particles. Measurements were conducted both in the near field about 50-200 m behind the emitting aircraft in non-contrailforming conditions as well as in the far field >19 km behind the A350-900 in contrail-forming conditions (see Table S1), whereby the contrail conditions were identified by the temperature difference to T_{SA} and the measured ice number concentrations. In the near field, each test point lasted about 45 s and was repeated at least five times; in the far-field, each test point was measured for 20 min, with multiple background measurement sequences in between.

Aerosol number emission indices from fuels with different sulfur contents

Figure 3a shows the emission index of volatile particles (vPM) and non-volatile particles sampled during near-field measurements at FL310 (9465 m

Fig. 3 | Emission indices of volatile particles and non-volatile particles. Number of volatile particles >5 nm (circles) and non-volatile particles >14 nm (diamonds) per kg fuel burned measured at 9465-9730 m altitude. Measurements were performed in the near field in the 0.5-2 s old exhaust in non-contrail-forming conditions 2 K above T_{SA} and RHi below 60% (a), and in the far field in contrailforming conditions in the 50-300 s old contrail at air temperatures 9-10 K below T_{SA} and RHi of 70-100% (b). The figure shows median values and 25th-75th percentiles of the emission index for the ultra-low-sulfur HEFA-SPK (green), the low-sulfur Jet A-1 (dark gray), and the medium-sulfur blend fuel (blue); gray dots represent data from single exhaust crossings.



altitude) at medium T30³³. Measurements were conducted in non-contrail-forming conditions, with atmospheric temperatures above the Schmidt-Appleman threshold temperature (see Table S1). Aerosols are therefore not influenced by the formation of ice particles. It is clearly visible that in the young plume of the RQL combustor the majority of the particles are non-volatile, presumably mostly soot particles. The number emission index of nvPM thereby correlates with the aromatic content of the fuel³³.

The number of volatile particles correlates with fuel sulfur content, with combustion of the quasi-sulfur-free HEFA-SPK producing the lowest number of vPM. The increasing number of volatile particles for the Jet A-1 with a sulfur content of 125 ppm and the blend fuel containing 505 ppm sulfur could therefore indicate that sulfuric compounds in the exhaust gas lead to an increased growth of ultrafine volatile aerosol, resulting in more particles reaching a diameter detectable by condensation particle counters (CPC). However, the growth of volatile particles might be limited by the low availability of water vapor resulting from the low RHi and high temperature in the near-field.

The emission indices of volatile and non-volatile particles in the far field at 1-3 min contrail age are shown in Fig. 3b and the statistical significance of the results is listed in Table S2. Those measurements were taken in contrail-forming conditions at atmospheric temperatures 9.5-10.5 K below the Schmidt-Appleman threshold temperature. Emissions of non-volatile aerosol are comparable to the near field for HEFA-SPK and Jet A-1 test points. The blend fuel shows increased nvPM numbers compared to non-contrail-forming conditions in the near field. This could be caused by contrail ice residuals that were not evaporated in the thermal denuder (see section "Contrail apparent ice emission indices from fuels with different sulfur contents"). Also, the measurement uncertainty is increased for the far-field. However, a similar trend of an increasing number of nvPM in contrails of several minutes age in the contrail dissipation phase has been observed previously with a different measurement system⁵⁶. It is therefore also conceivable that the ice phase leads to a processing of volatile material that is then no longer vaporized by the thermal denuder

The number of volatile particles from test points using Jet A-1 and HEFA-SPK is increased compared to the near-field sequences. Ion-mode particles are expected to grow until about an hour after the formation⁵³, therefore, it is likely that more of these particles now contribute to the detectable volatile aerosol in the far field. Due to the scatter in the data, the difference between both fuels is classified as not statistically significant (see Table S2). While we attempt to provide an explanation for the observations, comparisons of vPM from the combustion of HEFA-SPK and Jet A-1 should therefore be interpreted cautiously: despite the different sulfur contents, both fuels produce, within the uncertainty range, a similar amount

of volatile aerosol. This observation is consistent with previous model results and experiments ^{32,53}. These suggest that for a sulfur content below about 100 ppm, the number of volatile particles is mainly determined by the chemiion concentration and the condensation of organic compounds rather than the fuel sulfur content. Measurements of Jet A-1 were up to 100 s younger, so the volatile aerosol had less time to grow than in the HEFA-SPK case, which could explain the lower vPM EI for Jet A-1 compared to HEFA-SPK in the far field.

Particularly striking is the twentyfold increase in volatile particles at low temperature compared to the near field at warmer temperatures when using the medium-sulfur blend fuel. In the near field, the growth of volatile aerosols is restricted due to the shorter development time, higher temperature, and lower relative humidity. As described in the section "Exhaust particles and contrail formation", in the far-field, the absorption of water vapor can lead to the formation of activation-mode as well as accumulation-mode particles. These particles reach sufficiently large diameters to be captured by the CPCs and could therefore make a substantial contribution to the number of detectable volatile aerosol.

In contrast, the observation of a moderate increase in volatile particles for HEFA-SPK and Jet A-1 indicates that hardly any volatile particles reach sufficiently large diameters to be detected by the CPCs, and to act as cloud droplet nuclei, preventing the formation of activation-mode and accumulation-mode aerosol.

Contrail apparent ice emission indices from fuels with different sulfur contents

Figure 4a shows the apparent ice emission index (AEI) from the far-field measurements. The number of contrail ice particles is largely dependent on relative humidity and temperature difference to $T_{\rm SA}^{57}$. Ice particles start to evaporate as soon as the RHi falls below 100%, with the evaporation rate increasing as the relative humidity decreases. We therefore classify the data according to the prevailing in-plume RHi at the time of measurement, acknowledging potential variations in RHi during plume evolution. Measurements burning HEFA-SPK and blend fuel on 25 November 2021 were performed in contrails of similar age, while contrails of Jet A-1 and HEFA-SPK on 24 November 2021 were 1-2 min younger. The age difference could result in a more advanced sublimation of the ice particles in sub-saturated conditions for the blend fuel compared to HEFA-SPK and Jet A-1 of the first far-field flight. Due to the scatter caused by the sub-saturated atmospheric conditions, no statistically significant conclusion can be drawn from the comparison of Jet A-1 and HEFA-SPK (see section "SM1 Measurement conditions" in the Supplementary information). Nonetheless, a significant increase in ice particle numbers can be seen when using the medium-sulfur blend fuel compared to HEFA-SPK and Jet A-1 at similar RHi.

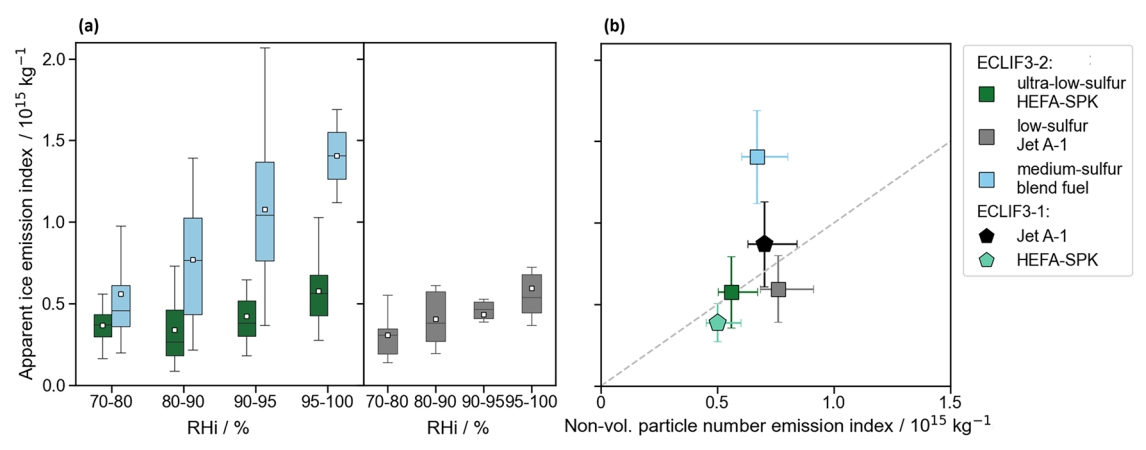


Fig. 4 | **Apparent ice emission indices (AEI) from contrail measurements.** a Ice particle number per kg of fuel burned using ultra-low-sulfur HEFA-SPK (green), low-sulfur Jet A-1 (dark gray), and medium-sulfur blend fuel (blue). Measurements were performed in the far field in the 50–300 s old contrail at 9620–9730 m altitude and air temperatures 9–11 K below $T_{\rm SA}$. Measurements sequences are divided according to the relative humidity over ice of the ambient air. Boxes extend from the first quartile to the third quartile of the data, with a black line indicating the median and white boxes indicating mean values. The whiskers extend to the maximum and minimum data points. Due to the scatter caused by the varying measurement conditions, no statistically significant conclusion can be drawn from the comparison

of Jet A-1 and HEFA-SPK. **b** Mean AEI from far-field (95% < RHi < 100%) vs nvPM emission indices from near-field measurements (squares), including uncertainty intervals. Differences in engine and combustor operating conditions between the near and far field can result in increased nvPM emissions in the far field (see the section "Particle and trace gas measurements"), as reflected by the extended error bars. Jet A-1 and HEFA-SPK test points from the earlier ECLIF3-1 campaign measured at supersaturated atmospheric conditions are shown as black and light-green pentagons, including uncertainty intervals according to Märk et al. and Dischl et al. ^{22,33}. The dashed line represents the 1:1 relationship between AEI and nvPM EI.

For Jet A-1 and HEFA-SPK, the apparent ice emission index corresponds, within the uncertainty range, to the emission index of soot particles from near field with about $5-8\times10^{14}$ particles per kg fuel burned (Fig. 4b). In this regime, the number of ice particles is well correlated to the number of soot particles. This correlation is evident for the largest RHi, while the evaporation of ice particles results in a visible decrease in ice particles for RHi below 95%.

The ice particle number exceeds the number of soot particles when burning the blend fuel. The mean apparent ice emission index for the relative humidity range of 95–100% amounts to 1.4×10^{15} particles per kg fuel burned, which is two times larger than the nvPM EI measured in the near field. With a volatile particle EI of 6×10^{15} per kg fuel burned (see Fig. 3b), about 10% of the volatile particles >5 nm additionally contribute to the formation of contrail ice particles. These results show that the contribution of volatile aerosol from sulfuric compounds to the formation of contrail ice particles is very likely for fuel sulfur contents over 500 ppm and the soot characteristics of the investigated engine and fuel. The number of ice particles decreases only slightly with decreasing RHi for Jet A-1 and HEFA-SPK, while the AEI for the blend fuel decreases strongly with relative humidity. This could indicate that at lower RHi, the ice particles formed on volatile particles remain smaller due to the limited availability of water vapor and therefore evaporate faster.

Figure 4b additionally shows AEIs and nvPM EIs from ECLIF 3-1 measurements, which investigated the same aircraft and engine type as in this study. Far-field AEI data are obtained from Märkl et al.²² and near-field nvPM EIs are published by Dischl et al.33. It should be noted that Märkl et al.22 derived nvPM EIs based on far-field measurements. For both fuels, the number of soot particles primarily determines the number of contrail ice particles, with deviations of up to 15% arising from additional, sulfur-related processes influencing ice nucleation: (1) Ice particle numbers exceed nvPM numbers from near-field measurements for the Jet A-1 burned during ECLIF3-1. The Jet A-1 fuel of ECLIF3-1 contained 211 ppm sulfur, indicating an onset of volatile particle contribution to ice crystal formation for a fuel sulfur content between 125 and 211 ppm for the probed engine. (2) In contrast, the AEIs observed for the ECLIF3-1 ultra-low-sulfur HEFA-SPK are lower than the corresponding nvPM EIs. Previous contrail observations at ice supersaturation^{21,45} also show a reduced number of soot particles acting as CN and therefore lower contrail ice crystal numbers for low sulfur fuels compared

to high-sulfur fuels. Due to these modulating effects of fuel sulfur on ice crystal numbers, the use of alternative fuels reduces the number of ice particles beyond the reduction in soot particle numbers: Measurements during ECLIF3-1 at supersaturated conditions showed a 35% reduction in soot particle numbers and a 56% reduction in ice particles numbers burning quasi-sulfur-free HEFA-SPK compared to a Jet A-1 fuel with 211 ppm sulfur content²².

Figure 5 shows normalized ice particle size distributions (PSD) of one representative plume crossing for each fuel measured at an in-plume RHi of about 95%. In addition to RHi and the temperature difference to T_{SA} , the contrail age and the difference between emission and detection altitude Δz should be taken into account when considering ice particle sizes²². Particle size distributions as a function of plume age and Δz are shown in Fig. S1. For Fig. 5 we selected one representative plume crossing of comparable RHi, $\Delta T_{\rm SA}$, Δz and plume age to apply log-normal fit functions (see the section "Particle size distribution") to the PSD of each fuel. Contrails of measurements burning Jet A-1 were slightly younger and at higher Δz , which could lead to a deviation in the distribution of small ice particles. The maximum of the size distributions of all fuels is evident at a particle diameter of about 1.6 µm, likely caused by nucleation of ice particles on soot. However, in contrast to the quasi-sulfur-free HEFA-SPK, particle size distributions of Jet A-1 and blend fuel exhibit an additional, smaller particle mode at about 1 μm. For the blend fuel, the maximum number concentration of that small mode is twice as large compared to that of Jet A-1. The occurrence of the smaller mode for the Jet A-1 fuel could indicate the onset of ice activation of volatile particles, which is, however, not yet reflected in increased ice particle number concentrations.

Modeling of aerosol emissions and contrails

The results demonstrate that the combustion of fuels with medium sulfur content can lead to an increasing ice activation of volatile aerosols, even with modern RQL combustors. In-flight measurements can only capture the limited range of nvPM emissions from the test aircraft; therefore a model is used to simulate the apparent ice emission indices for the three different fuels and varying nvPM number emissions. Figure 6 shows the dependence of the apparent ice emission index on nvPM EI numbers, as simulated by the Aerosol and Contrail Microphysics (ACM) model (see the section "ACM model"). For high nvPM emissions exceeding 10¹⁵ particles per kg of fuel, a

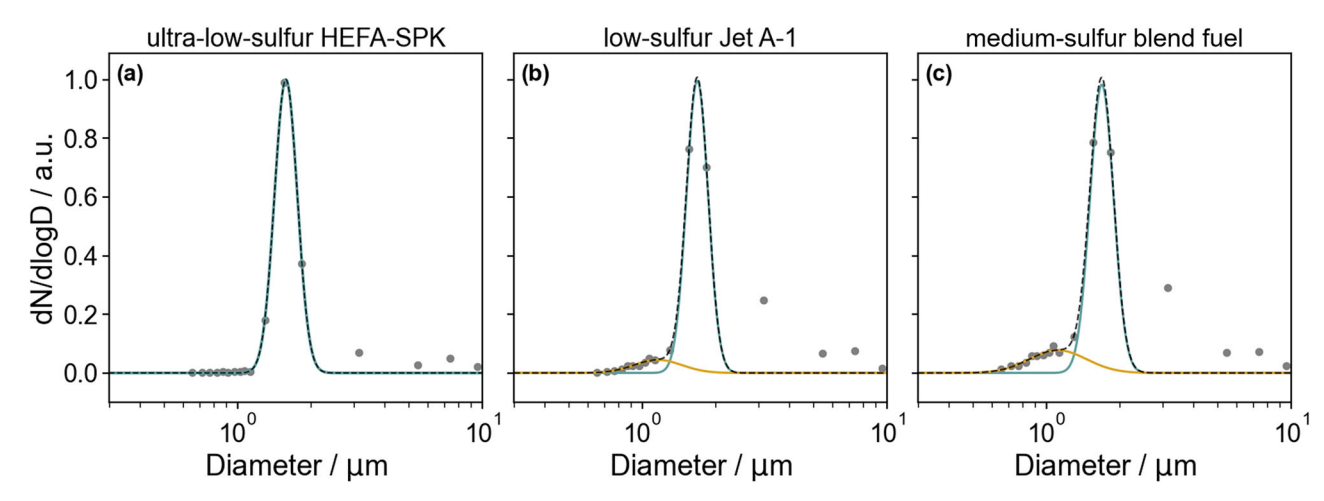


Fig. 5 | Ice particle size distribution (PSD) of representative contrail crossings from HEFA-SPK, Jet A-1 and blend fuel. PSDs (gray dots) of a HEFA-SPK, b Jet A-1, and c blend fuel are normalized with respect to the maximum of the log-normal fit function of the main mode (blue). Low-sulfur Jet A-1 and medium-sulfur blend fuel contrail PSDs show two modes, a larger main (blue) and additionally a smaller

secondary particle mode (yellow). The envelope (dashed black) represents the overall distribution. Ice particles larger than 3 μm have been observed previously 9,87 and can potentially be assigned to ice particles from surrounding cirrus clouds and larger contrail ice particles.

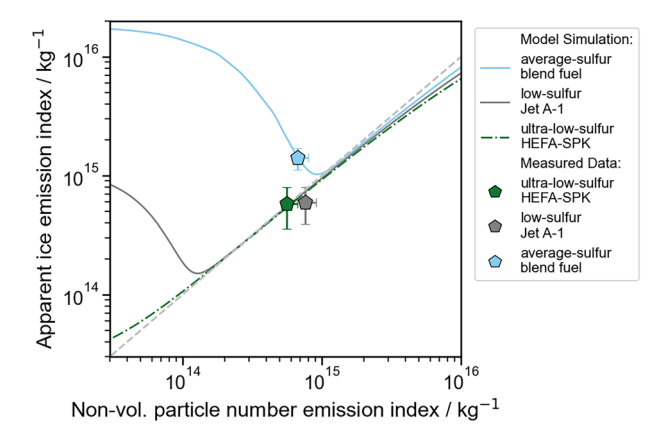


Fig. 6 | Dependence of the apparent ice emission index on the nvPM emission index. Dependence of contrail AEI on nvPM EI (lines) at 100% RHi for the tested fuels, as simulated by the ACM model. Symbols represent mean AEI from far-field (95% < RHi < 100%) vs. nvPM emission indices from near-field measurements, including uncertainty interval. The gray dashed line represents the 1:1 relationship between AEI and nvPM EI.

1:1 dependence is modeled between the number of contrail ice particles and nvPM for all fuels. For lower nvPM EI, the medium-sulfur blend fuel shows an increase in ice particles with decreasing nvPM under the given ambient temperature due to the activation of volatile aerosols acting as additional condensation nuclei. Therefore, ice particle numbers can exceed soot particle numbers for this fuel, as observed during the measurements. Reducing the fuel sulfur content can shift this limit to lower nvPM numbers. For the low-sulfur Jet A-1, a contribution from volatile aerosols is predicted below 10¹⁴ non-volatile particles per kg of fuel. A further reduction in sulfur content close to zero, as for HEFA-SPK, could strongly reduce the contribution of volatile aerosol to ice formation. It is important to note that the current ACM model does not account for organic compounds^{47,58} or lubrication oil^{59,60}. Their contribution could enhance the growth and activation of volatile particles, which is not considered in the simulations. Including these compounds may shift the onset of volatile particle activation to higher nvPM number EI, particularly at low FSC⁵⁴.

Discussion

For measurements close to the engine exit, we observe a dependence of volatile aerosol numbers on fuel sulfur content. The medium-sulfur blend

fuel produces the largest number of volatile aerosols, and the ultra-lowsulfur HEFA-SPK produces the lowest number of volatile aerosols for measurements below 60% RHi and an air temperature 2 K above $T_{\rm SA}$. During measurements in contrails in colder ambient temperatures $(\Delta T_{\rm SA} \approx -10 \,\text{K} \text{ and } 70\% < \text{RHi} < 100\%)$ a significant increase in volatile particle numbers is observed for the medium-sulfur blend fuel, which is not detected for either of the other fuels with lower sulfur contents. The increased sulfur content of the blend fuel likely causes the growth of volatile aerosol particles, resulting in particle sizes >5 nm and therefore large enough to be measured by the CPCs. Through this growth, the volatile particles eventually become large enough to serve as cloud droplet nuclei, leading to the formation of additional contrail ice crystals. While the number of ice particles for ultra-low-sulfur HEFA-SPK and low-sulfur Jet A-1 correlates with the number of nvPM, the ice particle number for the medium-sulfur blend fuel exceeds the number of nvPM by a factor of 2 and can be explained by the activation of about 10% of volatile particles larger than 5 nm. We observe an increasing influence of FSC on ice particle numbers for larger RHi. Further measurements are needed to determine whether this trend continues for RHi >100%, and to what extent the atmospheric temperature affects the activation of sulfate aerosols as ice nuclei.

As demonstrated in previous studies³³, near-field nvPM emission indices correlate with the hydrogen and aromatic content of the fuels, with the low-sulfur Jet A-1 fuel in this study showing the lowest hydrogen and the highest aromatic content. However, the highest ice particle numbers are observed for the medium-sulfur blend fuel, indicating that under these conditions, the ice activation of volatile sulfate aerosols can outweigh the contribution from soot particles.

The study covers fuel sulfur contents typically found in current and anticipated future jet fuels. Since the impact of fuel sulfur is strongly influenced by the number and potentially by the size characteristics of the soot particles⁵⁴, it also depends on the engine design. By testing Rolls-Royce Trent XWB-84 RQL engines, we examined a modern engine with a combustor technology that is widely used in current commercial aviation. However, flight experiments are inherently limited in the number of fuels, engine types, combustor designs, and atmospheric conditions that can be tested, introducing a larger variability than covered by this study. Expanding the scope through additional in-flight and ground measurements would be valuable. To address these limitations and broaden the applicability of our findings, we included model simulations for validation of our measurement results and extension to a broader range of nvPM number emissions. Modeling the dependence of ice particle numbers on nvPM EI for the three

fuels supported the observations: The combustion of fuels with medium sulfur content leads to the activation of volatile aerosols for engines with nvPM emissions below 10¹⁵ particles per kg of fuel, resulting in an increase in contrail ice particle numbers. For engines with higher nvPM emissions, nvPM and ice particle numbers scale linearly, which explains why this effect has not been observed previously for engines that emit more soot particles²¹. For low-sulfur fuels, volatile particles are activated at lower nvPM levels. Emissions of organic compounds and lubrication oil were not included in the modeling; depending on the emission location and mechanisms, these compounds could lead to larger volatile aerosols, potentially shifting the tipping points towards higher nvPM numbers.

When investigating the measured ice particle size distribution, we observe a main ice crystal mode at 1.6 μm for all fuels. The sulfur-containing Jet A-1 and blend fuels additionally show a smaller mode at 1.0 μm . The origin of this additional mode might be explained by the formation of volatile cloud droplet nuclei from sulfuric compounds in the aircraft plume. These volatile particles first have to grow in the plume, while soot particles are immediately available as ice nuclei. Therefore, the abundance of condensable water vapor is larger for droplets forming on soot particles, explaining the smaller size and number of ice particles forming on volatile aerosols. Smaller ice particles are also the first to evaporate, which could explain the equalization of the AEI of the different fuels at low RHi in Fig. 4.

The fuel sulfur content, therefore, influences the number of contrail ice particles in two different ways: First, the fuel sulfur activates the soot particles and initiates a liquid coating, leading to an enhanced uptake of water vapor by the particles. The growth of coated soot particles to contrail ice crystals correlates with the fuel sulfur and aromatic content⁴⁵. Previously observed reductions in ice activation for a low-sulfur semisynthetic Fischer-Tropsch-based fuel and ultra-low-sulfur SAFs^{21,22,45} suggest a general trend toward reduced ice-nucleating efficiency of soot particles for ultra-low-sulfur fuels. However, we note that full soot activation can still occur despite low FSC, suggesting that other factors also influence ice particle formation. Second, our results show that a fraction of contrail ice particles from conventional jet fuels with a medium sulfur content of 500 ppm may be caused by volatile aerosols serving as ice nuclei in the cold and humid aircraft exhaust. Reducing the fuel sulfur content to 125 ppm has been shown to limit the growth of volatile particles and their activation into contrail ice particles for the tested engine type. For engines with a higher soot emission index and larger-sized soot particles, the limit is expected to shift towards higher fuel sulfur contents^{31,45,54}.

Conclusion and outlook

By reducing the sulfur content of aviation fuels in modern aircraft engines, the number of contrail ice particles, and thus also the radiative forcing of contrails, could be strongly reduced. Since sulfur in jet fuels solely originates from its fossil-derived components, reducing sulfur and aromatic content either through the use of neat or blended HEFA-SPK, or via hydrotreatment of fossil jet fuels, has the potential to reduce contrail ice crystal numbers both by reducing the soot particle numbers and their ice nucleation efficiency, as well as the activation of volatile particles.

Our results can be used to further develop process models to take into account the partitioning between sulfur and soot particles and the related contrail ice formation⁶¹. Contrail⁶² and climate models^{17,24,63} could also be further developed to take into account the combined effect of sulfur and soot on contrail ice crystals and the resulting contrail radiative forcing. Our findings should be further explored through additional observations.

Lean combustion technologies reduce the number of soot particles by several orders of magnitude³⁴. Hence, hardly any soot particles are available as nuclei for contrail formation. This could strongly increase the relevance of volatile aerosols for the formation of contrail ice particles⁵⁴. A reduction in FSC also leads to a reduction in volatile aerosol emissions during taxi, takeoff, and landing at the airport on the ground and therefore can have positive effects on airport air quality^{64,65} and reduce the impact of SO₂ on public health⁶⁶. However, potential adverse effects^{5,6}, such as sulfate aerosol-radiation interaction as well as an increase in albedo of low clouds with

increased sulfate aerosol emissions and thereby an enhanced cooling of low-level clouds^{67,68} must be considered to derive the total climate impact from the fuel sulfur effects. A comprehensive understanding of these interactions is crucial for future regulatory frameworks.

Methods

Source aircraft and engines

The source aircraft, an Airbus A350-900 (Reg. F-XWB) was equipped with two latest-generation Rolls-Royce Trent XWB-84 engines. Since the engines of the A350-900 can be fed from separate fuel tanks, test flights with up to three different fuels could be accomplished to ensure comparable atmospheric and engine conditions. As the main parameter for determining the engine state, the combustor inlet temperature (*T*30) was used. In cruise conditions at constant altitude, *T*30 is linearly correlated with the fuel flow (FF)³³. The *T*30 setting for the measurements corresponds to standard cruise conditions.

The Trent XWB-84 engine uses a modern rich-burn/quick-quench/lean-burn (RQL) combustor. Currently, RQL combustors are the most common combustor type registered in the ICAO engine emissions database³⁴. RQL combustors employ a fuel-rich primary zone at the front end of the combustor. Downstream of the primary zone, the additional air required to complete the combustion process and reduce the gas temperature (quench) is injected to reach fuel-lean conditions at the combustor exit^{69,70}.

Fuel characteristics

During the flight tests, three different fuels were used: A conventional Jet A-1, a 38:62 blend of HEFA-SPK and conventional Jet A-1, and a 100 % HEFA-SPK SAF. Sustainable aviation fuels and blending of conventional jet fuel with SAF will become increasingly relevant in the future. The European Union plans a mandatory quota for sustainable aviation fuels up to \geq 70% SAF by 2050⁷¹ to comply with current climate targets. According to the strategy of the US Federal Aviation Administration (FAA), the US fuel industry is required to produce at least 3 billion gallons of SAF per year by 2030, and by 2050 100% of aviation fuel demand should be covered by SAF⁷².

Most of the current pathways to produce SAF lead to an aromatic-free fuel. Therefore, these sustainable aviation fuels currently need to be blended with conventional jet fuel to reach a minimum aromatic content of 8% by volume, which is considered to be the limit for drop-in fuels in current fuel specifications.

The conventional Jet A-1 fuel was provided by the local fuel supplier TotalEnergies at the Airbus site at Toulouse Blagnac airport. HEFA-SPK and the blend fuel were supplied by Neste Corporation; the blend fuel, therefore, did not contain the sampled Jet A-1, but was provided separately. Selected fuel properties are shown in Table 1. Fuel samples were collected from the aircraft tanks prior to the flights and analyzed according to ASTM standards ASTM3701 (hydrogen content), ASTM D5453 (sulfur content), and ASTM D6379 (aromatic content). The carbon content refers to the difference between 100% and the hydrogen and sulfur content. Compared to the global average Jet A-1, the sulfur content of the blend fuel is slightly larger, while the sampled Jet A-1 shows a decreased sulfur content. Naturally, HEFA-SPK contains no sulfur. Contamination during the supply chain or in the aircraft tank results in a low sulfur content of 3 ppm for the sampled HEFA-SPK.

Particle and trace gas measurements

The DLR research aircraft Dassault Falcon 20-E5 (Reg. D-CMET) was equipped with a comprehensive payload for measuring trace gases, aerosols, and ice particles. Aerosol and trace gas instruments received their sample air through inlets located at the upper fuselage in the center line of the aircraft.

The CO_2 concentration was measured with a non-dispersive infrared gas analyzer Licor-7000 (LI-COR Inc., Lincoln, NE, USA) and with a wavelength-scanned cavity ring-down spectrometer (CRDS, Picarro G2401-m, Picarro Inc., Santa Clara, CA, USA)⁵⁵.

Aerosol instrumentation includes five butanol-based condensation particle counters (CPC) measuring the number concentration of total particles with a lower 50% detection efficiency diameter (D_{50}) of 5 nm and non-volatile particles with a D_{50} of 14 nm³³. The number of volatile particles is determined by subtracting nvPM from the total particle numbers. The particle counters are based on TSI CPC model 3010 (TSI Inc., Minneapolis, USA) that have been modified for aircraft use in low-pressure environments. The non-volatile fraction is determined by sampling behind a thermodenuder set to 250 °C to remove all volatile particles from the sample stream. The particle measurements were calibrated with regard to decreasing counting efficiency in low-pressure environments, inlet line losses, and losses in the thermodenuder³³. The high flight velocity leads to sub-isokinetic sampling when measuring in contrail-forming conditions, resulting in ice particle enrichment in the inlet⁷³. The enrichment is dependent on the particle size, with enrichment factors ranging from 1.2 to 1.3 for ice particle sizes between 1 and 2 µm. Since the fraction of particles enclosed in ice crystals can vary considerably between different aerosol species and would only be an estimate, no correction for the inlet enrichment was applied to particle numbers. The uncertainty of the particle measurements is 7-13% for an air pressure between 250 and 350 hPa, arising mainly from uncertainty of the low-pressure correction functions³³.

Differences between measurement conditions in the near and far field can result in increased nvPM emissions in the far field, attributed to different engine and combustor operating conditions. Modeling particle numbers using the MEEM model⁷⁴ results in an approximate 20% increase in nvPM EI in the far field, covered by extended error bars in Figs. 4b and 6.

Ice particle size and number are measured using a cloud and aerosol spectrometer (CAS) 75 . Ice particle numbers are additionally measured using a cloud, aerosol, and precipitation spectrometer (CAPS). The instruments operate with a $\lambda=658$ nm laser. Forward-scattered laser light indicates information on ice particle size distribution and number concentration. The CAS covers a particle size range of 0.66–41 μm and CAPS covers a particle size range of 0.5–51 μm , therefore covering ice particle sizes typically observed in contrails. CAS (CAPS) is mounted on the port-side (starboard) inner-underwing position, resulting in a horizontal distance of $\sim\!2.7$ m and a vertical distance of about 2.8 m between cloud particle probes and aerosol or trace gas inlet, and a horizontal distance of about 5.3 m between the two cloud particle probes.

Atmospheric cruise conditions

Aircraft particle emissions were measured in the near field and in the far field along the French Atlantic coast at flight altitudes between 9400 and 9800 m. Near-field measurements were conducted about 50-200 m (plume age of about 0.5-2 s) behind the source aircraft in order to probe the unprocessed particle and trace gas emissions in non-contrail-forming conditions. Therefore, during the near-field test flight, the air temperature was 2 K above T_{SA} and at low RHi below 60% to prevent the formation of contrail ice crystals that could lead to the processing of aerosol particles through the contrail ice. Aerosol and ice particles in fully developed contrails were sampled in the far field at a distance between 11 and 80 km (plume age of about 50-300 s) behind the A350-900 at air temperatures 9-11 K below $T_{\rm SA}$ and RHi of 70–100%. Sub-saturated conditions lead to evaporation of the contrail ice. It is therefore important to compare measurements at similar RHi and contrail age. Information on RHi is only available for the time of the measurements. Deviations prior to the measurement time could impact the development of aerosols and ice crystals, leading to an increased uncertainty in the number concentrations of the humidity bins.

Further information on ambient conditions and engine settings is provided in Table S1.

Calculation of the Schmidt-Appleman threshold temperature

The Schmidt–Appleman threshold temperature $T_{\rm SA}$ defines the ambient air temperature below which water vapor condenses in the aircraft plume, enabling the formation of contrail ice particles. The temperature was calculated following an approach by U. Schumann⁷; a detailed description of

the calculation approach is provided by Dischl et al. ⁷⁶. For ambient temperature and pressure, measurements from the A350 were used, with an uncertainty of 0.5 K and 0.5 hPa, respectively. Water vapor data was obtained from the airborne mass spectrometer AIMS ⁷⁷ with an uncertainty of 8–12% in water vapor mixing ratio. Overall, this yields an uncertainty in $T_{\rm SA}$ of about 0.2 K for the ambient conditions during the measurements (see Table S1).

Calculation of emissions indices

To account for inhomogeneities in the plume and mixing of exhaust air with ambient air, particle concentrations are analyzed using the emission index (EI). Since contrail ice particles are not directly emitted by the engines, but develop subsequently in the exhaust plume, the term apparent ice particle emission index (AEI) is used for ice particle data. CO₂ measurements were used as a tracer to calculate the emission indices to scale aerosol and ice particle numbers to the amount of fuel burned, providing a dilution-independent measure of emission:

(A)EI =
$$\frac{RT}{p} \cdot \frac{\Delta N}{(M(C) + \alpha M(H)) \cdot \Delta CO_2}$$
 (1)

where R is the ideal gas constant, T and p are standard temperature (273.15 K) and pressure (1013.25 hPa), α is the hydrogen-to-carbon molar ratio of the fuel, M(C) and M(H) are the molar masses of carbon and hydrogen, ΔCO_2 and ΔN are the background-subtracted peak areas of the recorded concentrations of CO_2 and (ice) particles at standard conditions during a plume encounter sequence. The emissions index has the unit number of (ice) particles per kg of fuel burned. The uncertainty of the emission index can be calculated using Gaussian error propagation

$$\Delta(A)EI = \sqrt{\left(\frac{d(A)EI}{dn_x}\right)^2 \left(\Delta n_x^2 + \Delta b g_n^2\right) + \left(\frac{d(A)EI}{dCO_2}\right)^2 \left(\Delta CO_2^2 + \Delta b g_{CO_2}^2\right) + \left(\frac{d(A)EI}{d\alpha}\Delta\alpha\right)^2}$$
(2)

comprising the uncertainty of the particle measurements Δn_x of 7–13% for an air pressure of 250–350 hPa arising from uncertainties of the correction functions³³, the uncertainty of the hydrogen-to-carbon molar ratio of the fuel $\Delta \alpha$ of 0.1%, the measurement uncertainty of the CO₂ instrumentation of 0.2 ppmv and the standard deviation of the CO₂ background Δbg_{CO_2} of 0.1–0.2 ppmv, as well as the standard deviation of the particle background Δbg_n of 5–10%. Due to the strong signal enhancements observed in trace gases and aerosol concentrations during near-field plume encounters, the particle measurement uncertainty is the dominant contributor to the absolute uncertainty, resulting in a Δ EI of about 10%. In the far field, plume signals are more diluted and less distinguishable from the background, resulting in a higher mean Δ EI of 18%, occasionally reaching up to 30%, but remaining well below the magnitude of the observed effects. The uncertainty of the AEI amounts to 24–33%²².

Particle size distribution

Two main modes of the apparent ice particle emission index distributions with particle size were fitted using a log-normal function of the form

$$\frac{\mathrm{d(AEI)}}{\mathrm{d[log}(D_p)]} = \frac{n_{Dp}}{\sqrt{2\pi}\sigma} \exp\left\{-\frac{\left[\log\left(\frac{D_p}{D_c}\right)\right]^2}{2\sigma^2}\right\}$$
(3)

where AEI is the apparent ice emission index, n_p is the total ice particle number in the respective size bin with mean particle diameter D_p , D_c is the geometric mean diameter of the distribution and σ is a fit coefficient related to the distribution width. To compare size ratios independent of absolute particle numbers, PSDs are normalized with respect to the maximum of the

Table 2 | Fit parameters including uncertainty of PSDs shown in Fig. 5

	HEFA-SPK Main mode	Blend fuel Main mode	Blend fuel Secondary mode	Jet A-1 Main mode	Jet A-1 Secondary mode
log(D _c)	0.501 ± 0.003	0.535 ± 0.001	0.18 ± 0.08	0.5303 ± 0.0004	0.20 ± 0.12
σ	0.112 ± 0.004	0.111 ± 0.005	0.27 ± 0.04	0.102 ± 0.004	0.22 ± 0.04

Table 3 | Measurement conditions during plume encounters of PSDs shown in Fig. 5

	Ultra-low-sulfur HEFA-SPK	Low-sulfur Jet A-1	Medium-sulfur blend fuel
Contrail age (s)	270	124	234
Ambient RHi (%)	94	94	95
ΔT_{SA} (K)	-9.8	-9.6	-10.3
Δz (m)	-49	-10	-45

fitted distribution. Fit parameters for PSDs of the main mode (blue) and the secondary mode (yellow), shown in Fig. 5, are listed in Table 2. Besides engine and fuel parameters, contrail ice particle sizes are mainly dependent on the atmospheric air temperature in terms of ΔT_{SA} , the relative humidity over ice, and the difference between detection altitude and emission altitude Δz^{22} . In Fig. 5, we therefore selected a representative plume crossing with comparable parameters for each fuel to ensure comparability of the PSD between the fuels (see Table 3). Measurements of burning Jet A-1 were performed in a slightly younger contrail with higher Δz , which could lead to a decrease in small ice particles²².

ACM model

The aerosol and contrail microphysics model (ACM)⁵⁴ is a parcel model simulating the aerosol microphysics, including kinetic nucleation⁷⁸ and contrail microphysics⁵⁴ in jet plumes. The model comprises three main aerosol types: soot particles, nucleated sulfuric acid particles, and background aerosols, covering dry particle diameters from 0.55 nm to 15 µm. The size distribution of soot particles (aggregates) is assumed to be log-normal, with a median diameter of 35 nm and a standard deviation of 1.6. The ratio of the sizes of primary soot particles to the effective sizes of soot aggregates is assumed to be 0.41⁵⁴. For the simulations, temperatures were set to match the measurement conditions, as detailed in Table S1. For HEFA-SPK, the flight on 25 November 2021 was used as a reference. The RHi was set to 100.5%. The simulations correspond to ice particles of an ~150-s-old contrail. The model accounts for the coalescence of inactivated aerosols with activated particles and incorporates the competition for water vapor among both liquid and ice-phase particles. Sulfuric acid particles are classified into neutral, positively charged, and negatively charged clusters or particles. The concentration of chemiions at the engine exit is assumed to be 109 cm⁻³, and the effect of ions/charges on the formation and growth of volatile particles is considered. Scavenging of sulfuric acid by soot and background aerosols, as well as liquid and ice-phase contrail particles, is explicitly tracked, distinguishing between direct condensation of H2SO4 and the coagulation of sulfuric acid particles with other aerosols or activated contrail particles. Organic compounds and lubrication oil are not yet considered. The plume dilution ratio was determined using a parameterization based on ref. 79. The ACM model has been documented in greater detail in earlier work⁵⁴.

Data availability

Number concentration time series, emission indices, and particle size distributions shown in this study are collected in the DLR data repository at https://halo-db.pa.op.dlr.de/mission/129(https://doi.org/10.17616/R39O0T)⁸⁰⁻⁸⁶.

Received: 30 April 2025; Accepted: 27 October 2025; Published online: 14 November 2025

References

- Lee, D. et al. The contribution of global aviation to anthropogenic climate forcing for 2000 to 2018. Atmos. Environ. 244, 117834 (2021).
- IATA. ReFuelEU Aviation Handbook. Technical Report, Montréal, QC, Canada (IATA, 2024).
- Navarrete, A., Pavlenko, N. & O'Malley, J. SAF Policy Scorecard: Evaluating State-level Sustainable Aviation Fuel Policies in the United States. Technical Report, ICCT https://theicct.org/wp-content/ uploads/2024/11/ID-225-%E2%80%93-SAF-scorecard_final.pdf (2024).
- Singh, D. K., Sanyal, S. & Wuebbles, D. J. Understanding the role of contrails and contrail cirrus in climate change: a global perspective. *Atmos. Chem. Phys.* 24, 9219–9262 (2024).
- Prather, M. J., Gettelman, A. & Penner, J. E. Trade-offs in aviation impacts on climate favour non-CO₂ mitigation. *Nature* 643, 988–993 (2025).
- Voigt, C. Solving aviation's climate-action conundrum. Nature 643, 921–923 (2025).
- Schumann, U. On conditions for contrail formation from aircraft exhausts. *Meteorol. Z.* 5, 4–23 (1996).
- 8. Kaufmann, S. et al. In situ measurements of ice saturation in young contrails. *Geophys. Res. Lett.* **41**, 702–709 (2014).
- 9. Voigt, C. et al. Extinction and optical depth of contrails. *Geophys. Res. Lett.* **38**, 1–5 (2011).
- Voigt, C. et al. ML-CIRRUS: the airborne experiment on natural cirrus and contrail cirrus with the high-altitude long-range research aircraft HALO. Bull. Am. Meteorol. Soc. 98, 271–288 (2017).
- Wang, Z. et al. Observations of microphysical properties and radiative effects of a contrail cirrus outbreak over the North Atlantic. *Atmos. Chem. Phys.* 23, 1941–1961 (2023).
- Sullivan, S. Clouds and their Climatic Impact: Radiation, Circulation, and Precipitation. No. 281 in Geophysical Monograph Series (American Geophysical Union, 2024).
- Burkhardt, U., Kärcher, B. & Schumann, U. Global modeling of the contrail and contrail cirrus climate impact. *Bull. Am. Meteorol. Soc.* 91, 479–484 (2010).
- Bock, L. & Burkhardt, U. Reassessing properties and radiative forcing of contrail cirrus using a climate model. *J. Geophys. Res.: Atmos.* 121, 9717–9736 (2016).
- Luo, H., Quaas, J. & Han, Y. Examining cloud vertical structure and radiative effects from satellite retrievals and evaluation of CMIP6 scenarios. Atmos. Chem. Phys. 23, 8169–8186 (2023).
- Teoh, R. et al. Targeted use of sustainable aviation fuel to maximize climate benefits. *Environ. Sci. Technol.* 56, 17246–17255 (2022).
- 17. Gettelman, A. et al. The future of Earth system prediction: advances in model-data fusion. Sci. Adv. 8, eabn3488 (2022).
- Beyersdorf, A. J. et al. Reductions in aircraft particulate emissions due to the use of Fischer–Tropsch fuels. *Atmos. Chem. Phys.* 14, 11–23 (2014).
- Schripp, T. et al. Aircraft engine particulate matter emissions from sustainable aviation fuels: results from ground-based measurements during the NASA/DLR campaign ECLIF2/ND-MAX. Fuel 325, 124764 (2022).
- Moore, R. H. et al. Biofuel blending reduces particle emissions from aircraft engines at cruise conditions. *Nature* 543, 411–415 (2017).
- Voigt, C. et al. Cleaner burning aviation fuels can reduce contrail cloudiness. Commun. Earth Environ. 2, 114 (2021).

- Märkl, R. S. et al. Powering aircraft with 100% sustainable aviation fuel reduces ice crystals in contrails. *Atmos. Chem. Phys.* 24, 3813–3837 (2024).
- Burkhardt, U., Bock, L. & Bier, A. Mitigating the contrail cirrus climate impact by reducing aircraft soot number emissions. *npj Clim. Atmos.* Sci. 1, 37 (2018).
- Bier, A. & Burkhardt, U. Impact of parametrizing microphysical processes in the jet and vortex phase on contrail cirrus properties and radiative forcing. *J. Geophys. Res.: Atmos.* 127, 1–29 (2022).
- Fahey, D. W. et al. Emission measurements of the concorde supersonic aircraft in the lower stratosphere. Science 270, 70–74 (1995).
- Kärcher, B. & Fahey, D. W. The role of sulfur emission in volatile particle formation in jet aircraft exhaust plumes. *Geophys. Res. Lett.* 24, 389–392 (1997).
- Yu, F. & Turco, R. P. The role of ions in the formation and evolution of particles in aircraft plumes. *Geophys. Res. Lett.* 24, 1927–1930 (1997).
- Schumann, U. et al. Pollution from aircraft emissions in the North Atlantic flight corridor: overview on the POLINAT projects. *J. Geophys. Res.: Atmos.* 105, 3605–3631 (2000).
- Toon, O. B. & Miake-Lye, R. C. Subsonic aircraft: contrail and cloud effects special study (SUCCESS). *Geophys. Res. Lett.* 25, 1109–1112 (1998).
- Hunton, D. E. et al. Chemical ionization mass spectrometric measurements of SO₂ emissions from jet engines in flight and test chamber operations. *J. Geophys. Res.: Atmos.* 105, 26841–26855 (2000).
- Petzold, A. et al. Near-field measurements on contrail properties from fuels with different sulfur content. *J. Geophys. Res.: Atmos.* 102, 29867–29880 (1997).
- Schumann, U. et al. Influence of fuel sulfur on the composition of aircraft exhaust plumes: the experiments SULFUR 1-7. J. Geophys. Res.: Atmos. 107, AAC 2–1 (2002).
- Dischl, R. et al. Measurements of particle emissions of an A350-941 burning 100% sustainable aviation fuels in cruise. *Atmos. Chem. Phys.* 24, 11255–11273 (2024).
- ICAO. ICAO Aircraft Engine Emissions Databank. Technical Report, EASA, Montréal, QC, Canada https://www.easa.europa.eu/en/ domains/environment/icao-aircraft-engine-emissions-databank (2024).
- Hadaller, O. & Johnson, J. World Fuel Sampling Program. CRC Report No. 647. Technical Report (Coordinating Research Council, 2006).
- El. The Quality of Aviation Fuel Available in the United Kingdom Annual Survey 2016–2017. CRC/El Research report (Energy Institute, Coordinating Research Council, Inc., 2022).
- D02 Committee. Specification for Aviation Turbine Fuels http://www.astm.org/cgi-bin/resolver.cgi?D1655-22 (2022).
- Yu, F. & Turco, R. P. Contrail formation and impacts on aerosol properties in aircraft plumes: effects of fuel sulfur content. *Geophys. Res. Lett.* 25, 313–316 (1998).
- Kärcher, B. et al. Physicochemistry of aircraft-generated liquid aerosols, soot, and ice particles: 2. Comparison with observations and sensitivity studies. *J. Geophys. Res.: Atmos.* 103, 17129–17147 (1998).
- 40. Curtius, J., Arnold, F. & Schulte, P. Sulfuric acid measurements in the exhaust plume of a jet aircraft in flight: Implications for the sulfuric acid formation efficiency. *Geophys. Res. Lett.* **29**, 17–1 (2002).
- Jurkat, T. et al. Measurements of HONO, NO, NO, NO_y and SO₂ in aircraft exhaust plumes at cruise. *Geophys. Res. Lett.* 38, 1–5 (2011).
- Khou, J., Ghedhaïfi, W., Vancassel, X., Montreuil, E. & Garnier, F. CFD simulation of contrail formation in the near field of a commercial aircraft: effect of fuel sulfur content. *Meteorol. Z.* 26, 585–596 (2017).
- 43. Kärcher, B. Formation and radiative forcing of contrail cirrus. *Nat. Commun.* **9**, 1824 (2018).

- Petzold, A. et al. On the effects of organic matter and sulphurcontaining compounds on the CCN activation of combustion particles. *Atmos. Chem. Phys.* 5, 3187–3203 (2005).
- Jones, S. H. & Miake-Lye, R. C. Contrail modeling of ECLIF2/ND-MAX flights: effects of nvPM particle numbers and fuel sulfur content. *Meteorol. Z.* 33, 35–41 (2024).
- 46. Klemm, R. F. & Blades, A. T. Ionization in hydrocarbon flames. *Nature* **212**, 920–921 (1966).
- Yu, F., Turco, R. P. & Kärcher, B. The possible role of organics in the formation and evolution of ultrafine aircraft particles. *J. Geophys. Res.: Atmos.* 104, 4079–4087 (1999).
- Arnold, F. et al. Chemiion concentration measurements in jet engine exhaust at the ground: Implications for ion chemistry and aerosol formation in the wake of a jet aircraft. *Geophys. Res. Lett.* 27, 1723–1726 (2000).
- 49. Haverkamp, H., Wilhelm, S., Sorokin, A. & Arnold, F. Positive and negative ion measurements in jet aircraft engine exhaust: concentrations, sizes and implications for aerosol formation. *Atmos. Environ.* **38**, 2879–2884 (2004).
- Sorokin, A. Gaseous SO₃ and H₂SO₄ in the exhaust of an aircraft gas turbine engine: measurements by CIMS and implications for fuel sulfur conversion to sulfur (VI) and conversion of SO₃ to H2SO₄. Atmos. Environ. 38, 449–456 (2004).
- Schröder, F. et al. In situ studies on volatile jet exhaust particle emissions: Impact of fuel sulfur content and environmental conditions on nuclei mode aerosols. *J. Geophys. Res.: Atmos.* 105, 19941–19954 (2000).
- Kärcher, B. & Meilinger, S. K. Perturbation of the aerosol layer by aviation-produced aerosols: a parametrization of plume processes. *Geophys. Res. Lett.* 25, 4465–4468 (1998).
- Kärcher, B. et al. A unified model for ultrafine aircraft particle emissions. J. Geophys. Res.: Atmos. 105, 29379–29386 (2000).
- 54. Yu, F., Kärcher, B. & Anderson, B. E. Revisiting contrail ice formation: impact of primary soot particle sizes and contribution of volatile particles. *Environ. Sci. Technol.* **58**. 17650–17660 (2024).
- Harlass, T. et al. Measurement report: in-flight and ground-based measurements of nitrogen oxide emissions from latest-generation jet engines and 100% sustainable aviation fuel. *Atmos. Chem. Phys.* 24, 11807–11822 (2024).
- Anderson, B. E. et al. An assessment of aircraft as a source of particles to the upper troposphere. *Geophys. Res. Lett.* 26, 3069–3072 (1999).
- Bräuer, T. et al. Airborne measurements of contrail ice properties-"dependence on temperature and humidity. *Geophys. Res. Lett.* 48, e2020GL092166 (2021).
- Rojo, C., Vancassel, X., Mirabel, P., Ponche, J.-L. & Garnier, F. Impact of alternative jet fuels on aircraft-induced aerosols. *Fuel* 144, 335–341 (2015)
- Yu, Z. et al. Identification of lubrication oil in the particulate matter emissions from engine exhaust of in-service commercial aircraft. *Environ. Sci. Technol.* 46, 9630–9637 (2012).
- Ponsonby, J., King, L., Murray, B. J. & Stettler, M. E. J. Jet aircraft lubrication oil droplets as contrail ice-forming particles. *Atmos. Chem. Phys.* 24, 2045–2058 (2024).
- Kärcher, B. & Yu, F. Role of aircraft soot emissions in contrail formation. *Geophys. Res. Lett.* 36, L01804 (2009).
- 62. Teoh, R. et al. Global aviation contrail climate effects from 2019 to 2021. *Atmos. Chem. Phys.* **24**, 6071–6093 (2024).
- 63. Burkhardt, U. & Kärcher, B. Global radiative forcing from contrail cirrus. *Nat. Clim. Change* **1**, 54–58 (2011).
- Kapadia, Z. Z. et al. Impacts of aviation fuel sulfur content on climate and human health. Atmos. Chem. Phys. 16, 10521–10541 (2016).
- Grobler, C. et al. Marginal climate and air quality costs of aviation emissions. *Environ. Res. Lett.* 14, 114031 (2019).

- Dedoussi, I. C., Eastham, S. D., Monier, E. & Barrett, S. R. H. Premature mortality related to United States cross-state air pollution. *Nature* 578, 261–265 (2020).
- Righi, M., Hendricks, J. & Sausen, R. The global impact of the transport sectors on atmospheric aerosol: simulations for year 2000 emissions. *Atmos. Chem. Phys.* 13, 9939–9970 (2013).
- Gettelman, A. & Chen, C. The climate impact of aviation aerosols. *Geophys. Res. Lett.* 40, 2785–2789 (2013).
- 69. Lefebvre, A. H. & Ballal, D. R. Gas Turbine Combustion: Alternative Fuels and Emissions 3rd edn (CRC Press, 2010).
- Trivanovic, U. & Pratsinis, S. E. Opinion: eliminating aircraft soot emissions. *Aerosol Res.* 2, 207–223 (2024).
- Vilkas, G. 70% of Jet Fuels at EU Airports will have to be Green by 2050 [Press release] https://www.europarl.europa.eu/news/en/press-room/20230911IPR04913/70-of-jet-fuels-at-eu-airports-will-have-to-be-green-by-2050 (2023).
- FAA. Sustainable Aviation Fuels (SAF) https://www.faa.gov/about/ officeorg/headquartersoffices/apl/sustainable-aviation-fuels-saf (2024).
- Schöberl, M. et al. Characterization of the airborne aerosol inlet and transport system used during the A-LIFE aircraft field experiment. Atmos. Meas. Tech. 17, 2761–2776 (2024).
- Ahrens, D., Méry, Y., Guénard, A. & Miake-Lye, R. C. A New approach to estimate particulate matter emissions from ground certification data: the nvPM mission emissions estimation methodology. *J. Eng. Gas. Turbines Power* 145, 1–12 (2022).
- Baumgardner, D., Jonsson, H., Dawson, W., O'Connor, D. & Newton, R. The cloud, aerosol and precipitation spectrometer: a new instrument for cloud investigations. *Atmos. Res.* 59–60, 251–264 (2001).
- Dischl, R., Kaufmann, S. & Voigt, C. Regional and seasonal dependence of the potential contrail cover and the potential contrail cirrus cover over Europe. *Aerospace* 9, 485 (2022).
- Kaufmann, S. et al. The airborne mass spectrometer AIMS—Part 1: AIMS-H₂O for UTLS water vapor measurements. *Atmos. Meas. Tech.* 9, 939–953 (2016).
- Yu, F. et al. On nucleation pathways and particle size distribution evolutions in stratospheric aircraft exhaust plumes with H₂SO₄ enhancement. *Environ. Sci. Technol.* 58, 6934–6944 (2024).
- Schumann, U. et al. Dilution of aircraft exhaust plumes at cruise altitudes. Atmos. Environ. 32, 3097–3103 (1998).
- Voigt, C., Sauer, D. & Dischl, R. Dataset #10948 https://halo-db.pa.op. dlr.de/mission/129 (2025).
- 81. Voigt, C., Sauer, D. & Dischl, R. *Dataset #10947* https://halo-db.pa.op. dlr.de/mission/129 (2025).
- Voigt, C., Sauer, D. & Dischl, R. Dataset #10946 https://halo-db.pa.op. dlr.de/mission/129 (2025).
- 83. Voigt, C. & Märkl, R. *Dataset #10929* https://halo-db.pa.op.dlr.de/mission/129 (2025).
- Voigt, C. & Märkl, R. *Dataset #10931* https://halo-db.pa.op.dlr.de/ mission/129 (2025).
- Voigt, C. & Märkl, R. Dataset #10604 https://halo-db.pa.op.dlr.de/ mission/129 (2025).
- Voigt, C. & Märkl, R. *Dataset #10605* https://halo-db.pa.op.dlr.de/ mission/129 (2025).
- Voigt, C. et al. In-situ observations of young contrails overview and selected results from the CONCERT campaign. *Atmos. Chem. Phys.* 10, 9039–9056 (2010).

Acknowledgements

This work was supported by the DLR Aeronautics Research Program within the Project NEOFUELS, by the Deutsche Forschungsgemeinschaft DFG by

project no. 510826369 (ECOCON) and by the European Union's Horizon Europe program under grant no. 101192301 (A4CLIMATE). The article processing charges for this open-access publication were covered by the German Aerospace Center (DLR) within DEAL. F.Y. acknowledges funding support from the U.S. National Science Foundation (NSF) (AGS-2325458).

Author contributions

C.R., C.V., and M.G. coordinated the ECLIF3 project. C.R. and C.V. defined the test plan. C.V., S.K., A.D., and C.R. planned and coordinated the flight experiment. A.M., A.R., D.S., M.S., R.D., R.M., S.K., T.H., and V.H. performed the in-flight measurements. R.M. provided ice particle data. R.D. performed the measurement and test data evaluation and wrote the paper. F.Y. performed the model calculations. C.R., D.A., M.G., M.J., and P.S. assisted engine data interpretation. R.S. provided the fuels, and C.R., G.E., M.G., P.L.C., and R.S. performed fuel analyses. All authors contributed to the paper.

Funding

Open Access funding enabled and organized by Projekt DEAL.

Competing interests

M.J. and P.S. are employed by Rolls-Royce plc.; D.A. is employed by Rolls-Royce Deutschland; R.S. is employed by Neste Corporation. All other authors declare that they have no competing interests.

Additional information

Supplementary information The online version contains supplementary material available at https://doi.org/10.1038/s43247-025-02951-5.

Correspondence and requests for materials should be addressed to Rebecca Dischl.

Peer review information Communications Earth and Environment thanks Dharmendra Kumar Singh, Margaux Vals and the other, anonymous, reviewer(s) for their contribution to the peer review of this work. Primary Handling Editors: Nandita Basu and Yann Benetreau. A peer review file is available.

Reprints and permissions information is available at

http://www.nature.com/reprints

Publisher's note Springer Nature remains neutral with regard to jurisdictional claims in published maps and institutional affiliations.

Open Access This article is licensed under a Creative Commons Attribution 4.0 International License, which permits use, sharing, adaptation, distribution and reproduction in any medium or format, as long as you give appropriate credit to the original author(s) and the source, provide a link to the Creative Commons licence, and indicate if changes were made. The images or other third party material in this article are included in the article's Creative Commons licence, unless indicated otherwise in a credit line to the material. If material is not included in the article's Creative Commons licence and your intended use is not permitted by statutory regulation or exceeds the permitted use, you will need to obtain permission directly from the copyright holder. To view a copy of this licence, visit http://creativecommons.org/licenses/by/4.0/.

© The Author(s) 2025